https://doi.org/10.5194/cp-2023-83
Preprint. Discussion started: 8 November 2023

Climate of the Past Discussions

Highly stratified mid-Pliocene Southern Ocean in PlioMIP2

Julia E. Weiffenbach[1], Henk A. Dijkstra[1,2], Anna S. von der Heydt[1,2], Ayako Abe-Ouchi[3], Wing-Le Chan[3], Deepak Chandan[4], Ran Feng[5], Alan M. Haywood[6], Stephen J. Hunter[6], Xiangyu Li[7], Bette L. Otto-Bliesner[8], W. Richard Peltier[4], Christian Stepanek[9], Ning Tan[10], Julia C. Tindall[6], and Zhongshi Zhang[7,11]

[1]Institute for Marine and Atmospheric research Utrecht (IMAU), Department of Physics, Utrecht University, 3584 CC Utrecht, The Netherlands
[2]Centre for Complex Systems Science, Utrecht University, 3584 CE Utrecht, the Netherlands
[3]Atmosphere and Ocean Research Institute, University of Tokyo, Kashiwa, 277-8564, Japan
[4]Department of Physics, University of Toronto, Toronto, MS5S 1A7, Canada
[5]Department of Earth Sciences, College of Liberal Arts and Sciences, University of Connecticut, Storrs, CT 06033, USA
[6]School of Earth and Environment, University of Leeds, Woodhouse Lane, Leeds, West Yorkshire, LS2 9JT, UK
[7]Department of Atmospheric Science, School of Environmental Studies, China University of Geoscience, Wuhan, 430074, China
[8]National Center for Atmospheric Research, (NCAR), Boulder, CO 80305, USA
[9]Alfred-Wegener-Institut – Helmholtz-Zentrum für Polar und Meeresforschung (AWI), Bremerhaven, 27570, Germany
[10]Key Laboratory of Cenozoic Geology and Environment, Institute of Geology and Geophysics, Chinese Academy of Sciences, Beijing, 100029, China
[11]NORCE Norwegian Research Centre, Bjerknes Centre for Climate Research, 5007 Bergen, Norway

Correspondence: Julia E. Weiffenbach (j.e.weiffenbach@uu.nl)

Abstract. During the mid-Pliocene (3.264-3.025 Ma), atmospheric CO_2 concentrations were approximately 400 ppm and the Antarctic ice sheet was substantially reduced compared to today. Antarctica is surrounded by the Southern Ocean, which plays a crucial role in the global oceanic circulation and climate regulation. Using results from the Pliocene Model Intercomparison Project (PlioMIP2), we investigate Southern Ocean conditions during the mid-Pliocene with respect to the pre-industrial period. We find that the mean sea surface temperature (SST) warming in the Southern Ocean is 2.8°C, while global mean SST warming is 2.4°C. The enhanced warming is strongly tied to a dramatic decrease in sea-ice cover over the mid-Pliocene Southern Ocean. We also see a freshening of the ocean (sub)surface, driven by an increase in precipitation over the Southern Ocean and Antarctica. The warmer and fresher surface leads to a highly stratified Southern Ocean, that can be related to weakening of the deep abyssal overturning circulation. Sensitivity simulations show that the decrease in sea-ice cover and enhanced warming is largely a consequence of the reduction of the Antarctic ice sheet. In addition, the mid-Pliocene geographic boundary conditions are responsible for approximately half of the increase in mid-Pliocene SST warming, sea ice loss, precipitation and stratification increase over the Southern Ocean. From these results, we conclude that a strongly reduced Antarctic Ice Sheet during the mid-Pliocene has a substantial influence on the state of the mid-Pliocene Southern Ocean and exacerbates the changes that are induced by a higher CO_2 concentration alone. This is relevant for the long-term future of the Southern Ocean, as we expect melting of the western Antarctic ice sheet in the future, an effect that is not currently taken into account in future projections by CMIP ensembles.

https://doi.org/10.5194/cp-2023-83
Preprint. Discussion started: 8 November 2023

1 Introduction

The Southern Ocean is a critical component of the Earth's climate system as it acts as a major sink of heat and carbon dioxide (Khatiwala et al., 2009; Tjiputra et al., 2010; Iudicone et al., 2011) and affects global ocean circulation patterns (Talley, 2013; Rintoul, 2018). Close to the Antarctic margin, dense Antarctic bottom water (AABW) is formed that fills the abyssal ocean of the Atlantic and Indo-Pacific basins (Orsi et al., 1999; Johnson, 2008). Further north, strong westerly winds drive the upwelling of Circumpolar Deep Water (Marshall and Speer, 2012) and downwelling of Antarctic Intermediate Waters (Sloyan and Rintoul, 2001). The Southern Ocean circulation plays a vital role in mitigating the current rise of atmospheric CO_2 levels through its uptake of CO_2, where it is estimated that over 1999-2007 the Southern Ocean has taken up 40% of excess anthropogenic carbon present in seawater (Bopp et al., 2015). In addition, through its heat uptake the Southern Ocean modulates rising global air temperatures and ocean heat content (Frölicher et al., 2015; Liu et al., 2018).

While there have been several model studies concerning the impact of rising CO_2 levels on the future Southern Ocean (e.g., Ito et al., 2015; Bracegirdle et al., 2020; Almeida et al., 2021), these studies consider transient simulations following CMIP scenarios. Due to the absence of slow feedbacks, they cannot not inform us of the long-term impacts of higher CO_2 levels on the global and regional climate and typically do not take into account Antarctic ice sheet adjustment in a warming climate. One way to consider these effects is by studying warm paleoclimates during geological periods in which the atmospheric CO_2 concentration was similar to that of a possible near-future warm climate. One of these periods is the mid-Pliocene warm period (mPWP; 3.264-3.025 Ma). Burke et al. (2018) have shown that the near-future climate stabilized at the Representative Concentration Pathway 4.5 (RCP4.5) emission scenario is similar to the climate during the mPWP, and this period can therefore be considered a good geological analog for long-term future climate under moderate CO_2 emissions. The mPWP is the most recent geological period during which the CO_2 concentration was around 400 ppm (e.g., Seki et al., 2010; Pagani et al., 2010; de la Vega et al., 2020), which is close to present-day levels. The mPWP global mean surface temperature was ~ 3 degrees higher than during the pre-industrial (PI) (Haywood et al., 2013, 2020; McClymont et al., 2020). Geographic boundary conditions were also similar to present-day conditions, with some important differences including a substantially reduced Greenland Ice Sheet (Dolan et al., 2015), absence of the West Antarctic Ice Sheet, reduction of the East Antarctic Ice Sheet (Dowsett et al., 2010) and a different configuration of mostly high-latitude Northern Hemisphere (NH) ocean gateways, including the Bering Strait and Canadian Archipelago (Dowsett et al., 2016).

The Pliocene Model Intercomparison Project Phase 2 (PlioMIP2) encompasses an ensemble of 17 Earth System Models and was initiated to investigate the mPWP climate and to study its potential as a future climate analog (Haywood et al., 2016). Each participating model has provided at least a mPWP simulation (Eoi^{400}) and a PI simulation (E^{280}). The mPWP Eoi^{400} simulations are centered on an interglacial peak, the KM5c time slice at 3.205 Ma, during which orbital forcing was similar to present day. The mPWP boundary conditions, including orography, ice sheet extent and vegetation cover, are prescribed based on the reconstruction by the Pliocene Research, Interpretation and Synoptic Mapping (PRISM4) project (Dowsett et al.,

https://doi.org/10.5194/cp-2023-83
Preprint. Discussion started: 8 November 2023

2016). Previous studies using the PlioMIP2 ensemble have shown that surface temperature proxies generally agree well with the models (Haywood et al., 2020; McClymont et al., 2020) but that the boundary conditions, including orography, vegetation and ice sheet conditions, can have a strong regional influence on the simulated mPWP climate (Feng et al., 2022; Burton et al., 2023).

While the influence of orographic changes on the simulated mPWP climate can reduce the suitability of the mid-Pliocene as a geological analog for a future climate, the smaller ice sheet cover over Antarctica and Greenland during the mPWP can be very relevant for informing us on the impact of higher CO_2 levels combined with reduced ice sheet cover in the long-term future. In the Southern Hemisphere (SH) polar region, there are little orographic differences between the Eoi^{400} and E^{280} cases apart from those related to the reduced Antarctic ice sheet (Dowsett et al., 2016). It is therefore likely that the Southern Ocean in the mPWP simulations is primarily affected by a higher CO_2 level and the reduced Antarctic Ice Sheet cover. While the reconstructed ~ 24 m sea level equivalent of combined ice mass loss from the Greenland and Antarctic Ice Sheets in the mPWP (Haywood et al., 2016) seems unlikely for near-future scenarios, future projections on multi-centennial time scales do show substantial Antarctic Ice Sheet loss and potential West Antarctic Ice Sheet collapse under multiple climate scenarios (Cornford et al., 2015; Golledge et al., 2015; DeConto and Pollard, 2016; Bulthuis et al., 2019; Pattyn and Morlighem, 2020). Studying the state of the Southern Ocean in the mPWP simulations can therefore provide valuable insight into the impact of a reduced Antarctic Ice Sheet on both global and Southern Hemisphere ocean conditions in a warm equilibrium climate.

In this study, we will use model output from the PlioMIP2 ensemble to investigate Southern Ocean conditions during the mPWP. Our aim is to answer the following questions:

1. What are the differences between mPWP and PI states of the Southern Ocean and how do these impact the abyssal global ocean circulation?
2. How much do mPWP boundary conditions, primarily the reduced Antarctic Ice Sheet, contribute to the difference in Southern Ocean conditions between the mPWP and the PI and what are the resulting implications for a possible future climate?

To answer the first question, we will look at changes in Southern Ocean conditions in the mPWP compared to the PI in the PlioMIP2 models. This analysis includes sea-ice extent, temperature and salinity changes in the ocean, as well as atmospheric variables such as precipitation and wind that are first order controls on the oceanography of the Southern Ocean. We will then link changes in these variables to altered deep ocean circulation and ocean heat and salt transport in the Southern Ocean. For the second question, we consider 7 additional E^{400} sensitivity simulations of the ensemble. These simulations are in equilibrium at a mid-Pliocene CO_2 level, 400 ppm, but do not feature mPWP boundary condition changes. Using these sensitivity simulations, we assess to what extent sea-ice, temperature and salinity changes are influenced by a reduced Antarctic Ice Sheet.

https://doi.org/10.5194/cp-2023-83
Preprint. Discussion started: 8 November 2023

2 Methods

2.1 Data

We use datasets from simulations performed with 15 out of 17 models participating in PlioMIP2. NorESM-L and MRI-CGCM2.3 are excluded from this study because not all necessary data is available. Table 1 lists the 15 models used in this study along with their resolution and reference. Each of these models has completed one PI simulation (E^{280}) at approximately 280 ppm CO_2 and one mPWP simulation (Eoi^{400}) at 400 ppm CO_2 with mPWP boundary conditions that are described in Haywood et al. (2016). Additionally, 7 model groups have performed a sensitivity study where a PI simulation is performed at 400 ppm CO_2 (E^{400}). We use this simulation to separate the effect of increased CO_2 levels from that of other mPWP boundary conditions.

2.2 Analysis

We have used 100-year averages for all PlioMIP2 model fields except for IPSL-CM5A and IPSL-CM5A2. For the latter two models, we have used the available 50-year averages for E^{280} and Eoi^{400} experiments and a 30-year average for the E^{400} IPSL-CM5A2 experiment. Ocean freshwater and heat transport have been calculated on native model grids, except for COSMOS where computation is done on a regular interpolated 1×1 degree grid. All other variables are horizontally interpolated to a regular 1×1 degree grid, and any spatial averages presented in this study are calculated from these fields. Unless indicated otherwise, an anomaly is defined as Eoi^{400}–E^{280}, and any percentage anomalies are defined with respect to E^{280}.

The multi-model mean (MMM) is calculated by averaging over all the models in Table 1. The special model mean (SMM) is calculated by averaging over the 7 models that have E^{400} data. In Supplementary Figure S1, we compare the E^{280}, Eoi^{400} and Eoi^{400}–E^{280} SMM and MMM of surface variables used in this study. For the Southern Ocean, the SMM–MMM difference in the spatially averaged Eoi^{400}–E^{280} SST anomaly is approximately -0.5°C. The models included in the SMM therefore show substantially colder Southern Ocean SSTs than those included in the MMM. The difference in average sea surface salinity (SSS) anomaly is less than 0.1 psu. The location of the MMM and SMM sea-ice edge (15% sea-ice cover) is almost identical, although there are local differences in sea-ice cover between the SMM and MMM.

The stratification of the Southern Ocean is analyzed using the potential density ρ, which is calculated from potential temperature and salinity fields using the TEOS-10 equation of state (Roquet et al., 2015). To provide a measure for the stratification, we use the following stratification index (SI) following Bourgeois et al. (2022), based on Sgubin et al. (2017):

$$\mathrm{SI} = \sum_{i=1}^{10} \rho(z_i) - \rho(z_0) \tag{1}$$

where z_0 is the sea surface and $z_i = z_{i-1} + 200$ for $i = 1, \ldots, 10$ (units: m).

https://doi.org/10.5194/cp-2023-83
Preprint. Discussion started: 8 November 2023

Climate of the Past
Discussions
Open Access

Table 1. Overview of PlioMIP2 models used in this study. E^{400} sensitivity experiments have been provided by models typeset in bold.

Model name	Institute	Resolution		Reference
		Atmosphere	Ocean	
CCSM4	NCAR, USA	$0.9° \times 1.25°$, L26	$\sim 1° \times 1°$, L60	Feng et al. (2020)
CCSM4-UoT	University of Toronto, Canada	$0.9° \times 1.25°$, L26	$\sim 1° \times 1°$, L60	Peltier and Vettoretti (2014) Chandan and Peltier (2017)
CCSM4-Utr	IMAU, Utrecht University, The Netherlands	$2.5° \times 1.9°$, L26	$\sim 1° \times 1°$, L60	Baatsen et al. (2022)
CESM1.2	NCAR, USA	$0.9° \times 1.25°$, L30	$\sim 1° \times 1°$, L60	Feng et al. (2020)
CESM2	NCAR, USA	$0.9° \times 1.25°$, L32	$\sim 1° \times 1°$, L60	Feng et al. (2020) Feng et al. (2022)
COSMOS	AWI, Germany	$3.75° \times 3.75°$, L19	$3.0° \times 1.8°$, L40	Stepanek et al. (2020)
EC-Earth3-LR	Stockholm University, Sweden	$\sim 1.125° \times 1.125°$, L62	$1° \times 1°$, L46	Zhang et al. (2021)
GISS2.1G	GISS, USA	$2.0° \times 2.5°$, L40	$1° \times 1.25°$, L40	-
HadCM3	University of Leeds, UK	$2.5° \times 3.75°$, L19	$1.25° \times 1.25°$, L20	Hunter et al. (2019)
HadGEM3[1]	University of Bristol, UK	$1.875° \times 1.25°$, L85	$1° \times 1°$, L75	Williams et al. (2021)
IPSL-CM5A	LSCE, France	$3.75° \times 1.875°$, L39	$2.0° \times 2.0°$, $0.5°$ in the tropics, L31	Tan et al. (2020)
IPSL-CM5A2	LSCE, France	$3.75° \times 1.875°$, L39	$2.0° \times 2.0°$, $0.5°$ in the tropics, L31	Tan et al. (2020)
IPSL-CM6A	LSCE, France	$2.5° \times 1.26°$, L79	$\sim 1° \times 1°$, latitudinally refined at $1/3°$ in the equatorial region, L75	Lurton et al. (2020)
MIROC4m	JAMSTEC, Japan	$\sim 2.8° \times 2.8°$, L20	$1.4° \times 1.4°$, L43	Chan and Abe-Ouchi (2020)
NorESM1-F	NORCE, BCCR, Norway	$2.5° \times 1.9°$, L26	$\sim 1° \times 1°$, L30	Li et al. (2020)

[1] Pre-industrial land-sea mask in both simulations.

Averages for the Southern Ocean are calculated over all grid cells between 45°S-90°S, unless indicated otherwise. We calculate the Antarctic sea-ice area as the sum of the product of the sea-ice cover fraction and the grid cell area over all SH ocean grid cells. For Eoi^{400}, only grid cells that were also ocean grid cells in E^{280} were included in this analysis. Thus, any additional

https://doi.org/10.5194/cp-2023-83
Preprint. Discussion started: 8 November 2023

Climate of the Past Discussions

sea-ice that is formed in the mPWP in areas where the land-sea mask has changed from land to sea is not taken into account. This is to avoid bias in the sea-ice area anomaly due to ocean cells being created in locations where the Antarctic ice sheet has disappeared.

Furthermore, we use the following definitions for the Atlantic Meridional Overturning Circulation (AMOC) and the abyssal deep cell circulation: the AMOC strength is the maximum value of the Atlantic meridional overturning streamfunction at latitudes north of 0°N and below a depth of 500 m and the abyssal deep cell circulation strength is the absolute value of the most negative global meridional overturning streamfunction below a depth of 1000 m.

2.3 Results

2.3.1 Mid-Pliocene Southern Ocean in PlioMIP2

Figure 1a shows the MMM Eoi^{400}-E^{280} SST anomaly. The MMM global-average SST is 2.4°C warmer in the mPWP than in the PI while the Southern Ocean (45°S-90°S) is 2.8°C warmer. The ratio of SST warming in the Southern Ocean to global-average warming, the Southern Ocean SST amplification, is therefore 1.2. We can see regions of amplified warming more clearly in Figure 1b, which shows the MMM SST anomaly minus the MMM global-average SST anomaly. Warming amplification occurs in both the Northern and Southern Hemisphere at latitudes higher than approximately 40° in regions where sea-ice cover is absent in the Eoi^{400} simulations.

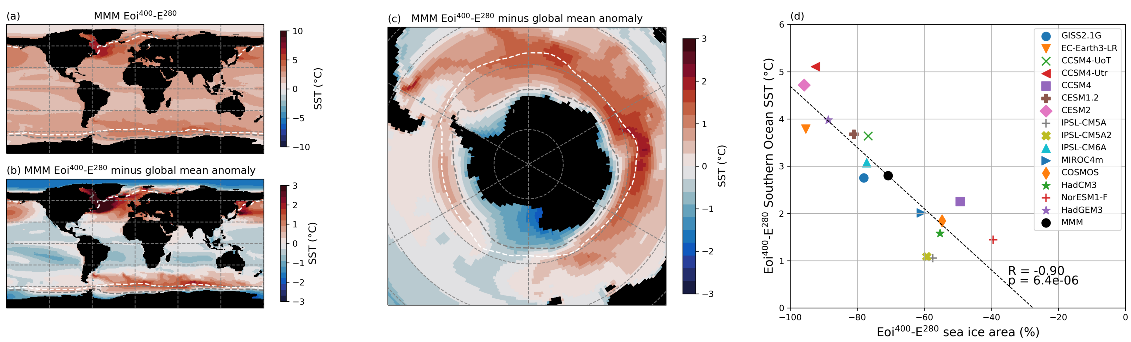

Figure 1. (a) MMM Eoi^{400}–E^{280} SST anomaly. (b) MMM Eoi^{400}–E^{280} SST anomaly minus the MMM global mean SST anomaly. (c) Same as (b) but on an orthographic projection centered on Antarctica. White and grey dashed lines show the MMM sea-ice edge (15% sea-ice cover) in E^{280} and Eoi^{400}, respectively. (d) Scatter plot of the individual model sea-ice area anomaly relative to E^{280} versus the SST anomaly in the Southern Ocean (45-90°S). Dashed line shows a linear least-squares fit,with indicated correlation R-value and p-value.

From Figure 1c, that focuses on the southern polar region, it is clear that the largest SST warming amplification in the Eoi^{400} simulations occurs around the pre-industrial sea-ice edge. In locations where sea-ice cover persists in the mPWP, the warming

https://doi.org/10.5194/cp-2023-83
Preprint. Discussion started: 8 November 2023

is at or below the global average. There is a strong correlation between the Southern Ocean temperature anomaly and sea-ice area decrease within the models ($R = -0.90$, $p < 0.05$, Figure 1d). Models with a relatively large decrease in sea-ice area generally also experience the highest SST warming in the Southern Ocean. Sea-ice reduction is therefore correlated to mPWP polar amplification in the Southern Hemisphere, although the analysis performed does not exclude the possibility that other mechanisms may be at work. Across the study ensemble, the MMM decrease in sea-ice area in the mPWP is 71% with respect to the pre-industrial sea-ice area.

Burton et al. (2023) show that higher mPWP CO_2 levels combined with the reduced albedo of the SH polar region are the main drivers behind the warming in this region. The 60°S-90°S-average annual-mean MMM SAT is 7.6°C higher than in the PI. Normalized by the MMM global-average SAT warming of 3.4°C, we find a SH polar amplification index of 2.2. This is substantially higher than both the CMIP6 abrupt-4xCO_2 SH polar amplification of 1.1 (centered around year-100) and the CMIP6 historical (1979-2014) SH polar amplification of 0.9 (Hahn et al., 2021), in which simulations are purely driven by fast feedbacks and ice sheet adjustments are not taken into account (Eyring et al., 2016). The amplified SAT warming over the majority of Antarctica and the high-latitude Southern Ocean (Supplementary Figure S2) likely contributes to the increase in precipitation over many parts of the SH polar region in the mPWP with respect to the PI (Figure 2a). The MMM increase in precipitation over the Southern Ocean and Antarctica is 0.35 mm day^{-1} (+14%) and 0.36 mm day^{-1} (+50%), respectively. Part of this increase in precipitation, particularly over the Southern Ocean, is offset by an equal or even larger increase in evaporation, as illustrated by the net surface freshwater flux anomaly in Figure 2b. Nevertheless, the net change in surface freshwater flux is still positive over the majority of the Southern Ocean, with a MMM increase in surface freshwater flux of 0.13 mm day^{-1} (+10%). We find that, as a result, the majority of the Southern Ocean becomes less saline at the surface, especially close to the Antarctic continent, and that this salinity decrease is robust across the PlioMIP2 ensemble (Figure 2c). The MMM change in Southern Ocean sea surface salinity (SSS) is -0.17 psu, with local minima down to -3.0 psu.

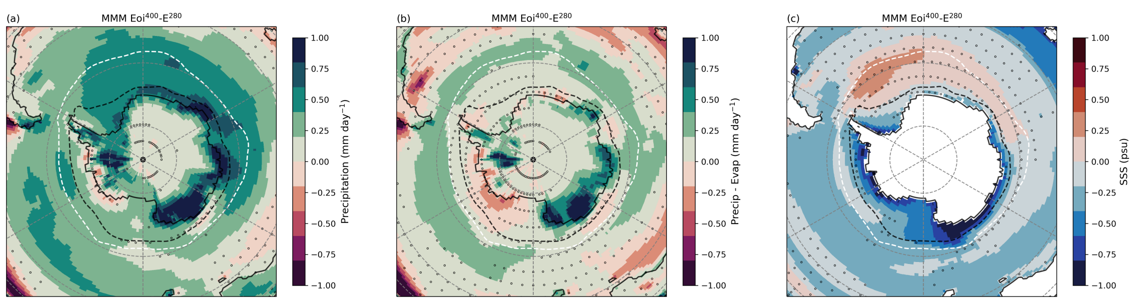

Figure 2. (a) MMM Eoi^{400}–E^{280} precipitation anomaly. (b) MMM Eoi^{400}–E^{280} surface freshwater flux (precipitation minus evaporation) anomaly. (c) MMM Eoi^{400}–E^{280} SSS anomaly. Stippling indicates that less than 12 out of 15 (<80%) of the models agree on the sign of change. White and black dashed lines show the MMM sea-ice edge (15% sea-ice cover) in E^{280} and Eoi^{400}, respectively.

https://doi.org/10.5194/cp-2023-83
Preprint. Discussion started: 8 November 2023

As Figure 1 and 2 show, the majority of the surface of the Southern Ocean both freshens and warms in the Eoi^{400} simulations with respect to E^{280}. It is inevitable that these changes affect the density stratification in the Southern Ocean. Figure 3a and b show the MMM Southern Ocean zonal-mean potential temperature and salinity anomalies, respectively. The warming is quite uniform throughout the water column apart from relatively low surface warming close to Antarctica and an increase in surface warming between approximately 45°S-65°S. In contrast, in the MMM zonal-mean salinity anomaly we see a clear pattern emerging that features a fresher ocean surface and saltier deeper ocean across all latitudes in the mid-Pliocene Southern Ocean. The same pattern is reflected in the MMM zonal-mean potential density anomaly in Figure 3c. In most models, we see a higher stratification in the mid-Pliocene Southern Ocean than in the pre-industrial (Supplementary Figure S3). At high latitudes (> 60°S), the increase in stratification is consistent across all PlioMIP2 ensemble members, as illustrated by their increase in high-latitude Southern Ocean stratification index (Figure 3d, Supplementary Table S1). The high-latitude Southern Ocean stratification index is defined as the average stratification index over all latitudes higher than 60°S, which is where abyssal deep water formation takes place. The gridded individual model stratification index anomalies are shown in Supplementary Figure S4. The MMM Eoi^{400}–E^{280} high-latitude Southern Ocean stratification index anomaly is 1.9 kg m^{-3}, corresponding to a relative increase of 37% with respect to the E^{280} MMM.

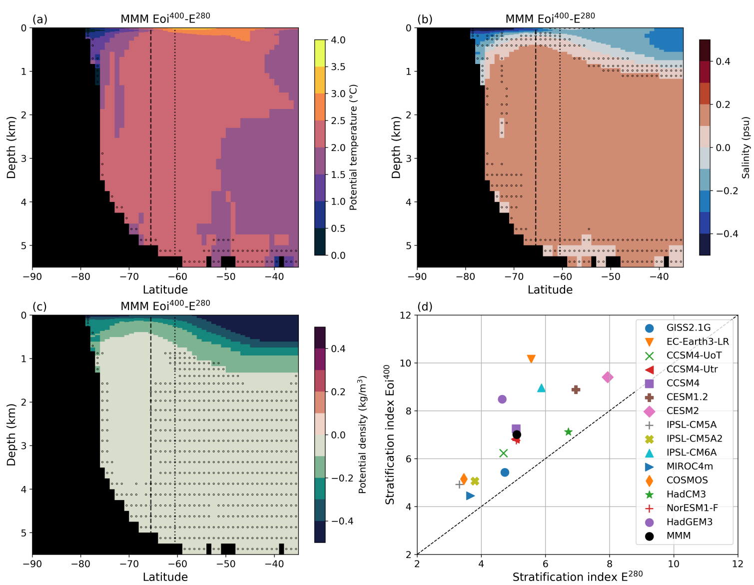

Figure 3. (a) MMM zonal mean Eoi^{400}–E^{280} potential temperature anomaly. (b) MMM zonal mean Eoi^{400}–E^{280} salinity anomaly. (c) MMM zonal mean Eoi^{400}–E^{280} potential density anomaly. Stippling indicates that less than 12 out of 15 (<80%) of the models agree on the sign of change. Vertical dotted and dashed lines indicate the MMM zonal mean sea-ice edge (15% sea-ice cover) in E^{280} and Eoi^{400}, respectively. (d) Scatter plot of the high-latitude Southern Ocean stratification index in E^{280} versus Eoi^{400}.

AABW formation is driven by buoyancy loss at the ocean surface. Consequently, the substantial increase in density stratifica-

https://doi.org/10.5194/cp-2023-83
Preprint. Discussion started: 8 November 2023

tion in high-latitude, non-circumpolar waters of the Southern Ocean is likely to have an impact on abyssal ocean circulation. Figure 4a shows the individual model and MMM Eoi^{400}–E^{280} anomalies of the AMOC and abyssal overturning strengths. Overall, we see a decrease in abyssal cell strength in 9 out of 15 models, with a MMM decrease of 2.5 Sv (-22%). The MMM AMOC strength increases by 3.1 Sv (+16%) in the mPWP simulations with respect to the PI. As 13 out of 15 models show a stronger mid-Pliocene AMOC, the response of the AMOC cell is more consistent than that of the abyssal cell.

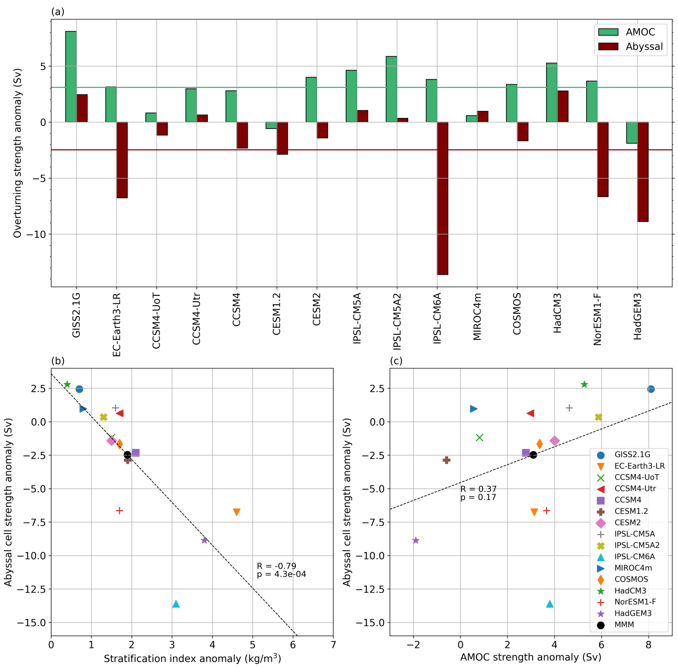

Figure 4. (a) Individual model Eoi^{400}–E^{280} AMOC and abyssal overturning strength anomalies. Horizontal lines indicate the MMM overturning strength anomalies. (b) Scatter plot of individual model Eoi^{400}–E^{280} Southern Ocean stratification index anomalies against the abyssal cell strength anomalies. (c) Scatter plot of individual model Eoi^{400}–E^{280} AMOC strength anomalies against the abyssal cell strength anomalies. Dashed lines show a linear least-squares fit to the individual model data, with indicated correlation R- and p-values.

The abyssal cell circulation strength should be related to the volume of deep water formation in the Southern Ocean, and therefore to surface water buoyancy in the high-latitude Southern Ocean. We find that the high-latitude ($> 60°$S) Southern Ocean stratification index anomaly shows a significant anti-correlation ($R = -0.76$, $p = 0.001$) with the abyssal cell strength anomaly (Figure 4b). The increased Southern Ocean stratification in the mid-Pliocene simulations therefore indeed appears to significantly impact the abyssal cell circulation and thereby the global ocean circulation. It is interesting, however, that the 6 models that do not feature a decrease in the abyssal cell strength still have a more stratified high-latitude Southern Ocean (Figure 4b). Figure 4c shows that 4 out of these 6 models do have the highest AMOC anomaly of the ensemble, which points to a possible interaction between the abyssal cell and the AMOC cell.

https://doi.org/10.5194/cp-2023-83
Preprint. Discussion started: 8 November 2023

When correlating the abyssal cell strength and the AMOC cell strength anomalies, there is no significant correlation (Figure 4d). However, when the outlier IPSL-CM6A is removed, the correlation does become significant ($R = 0.57$, $p = 0.03$). A possible explanation of this correlation is that when the abyssal waters return to the Southern Ocean, both by diapycnal upwelling to intermediate depths and by transport to the surface along isopycnals (Lumpkin and Speer, 2007), they interact with North Atlantic Deep Water (NADW) from the AMOC cell. In the Southern Ocean, wind-driven Ekman transport upwells NADW to the surface to ultimately return northward (Toggweiler and Samuels, 1995), but the majority of NADW is transformed to AABW (Talley, 2013; Rousselet et al., 2021). The stronger AMOC in the Eoi^{400} simulations is driven by more vigorous NADW formation due to increased salinity in the high North Atlantic (Weiffenbach et al., 2023). In this way, the higher volume of relatively saline NADW results in more AABW transformation, thereby partly compensating the effects of higher density stratification in the high-latitude Southern Ocean.

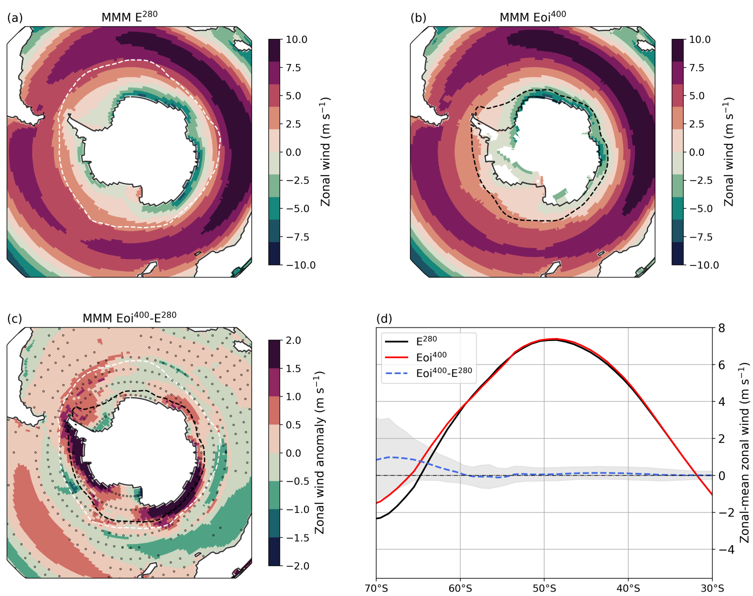

Figure 5. (a) MMM E^{280} 1000 hPa zonal wind, positive values indicate eastward wind. (b) MMM Eoi^{400} 1000 hPa zonal wind. (c) MMM Eoi^{400}–E^{280} 1000 hPa zonal wind anomaly. Stippling indicates that less than 12 out of 15 (<80%) of the models agree on the sign of change. White and black dashed lines show the MMM sea-ice edge (15% sea-ice cover) in E^{280} and Eoi^{400}, respectively. (d) MMM zonal-mean 1000 hPa zonal wind in Eoi^{400}, E^{280} and Eoi^{400}–E^{280}. Shading indicates one standard deviation around the MMM Eoi^{400}–E^{280} anomaly.

The pattern and strength of the zonal wind stress at the Southern Ocean surface also exert a strong effect on the global meridional overturning circulation through the wind-driven equatorward Ekman transport. Over the past decades, the westerly winds over the mid-latitude Southern Ocean have been strenghening and shifting polewards (Swart and Fyfe, 2012; Deng et al., 2022). An increase in strength and poleward shift of the mid-latitude Southern Hemisphere westerlies has also been shown under fu-

https://doi.org/10.5194/cp-2023-83
Preprint. Discussion started: 8 November 2023

ture warming scenarios (e.g., Kidston and Gerber, 2010; Bracegirdle et al., 2013). In PlioMIP2, we do not see any systematic changes in surface westerly winds over the Southern Ocean (Figure 5). Less than half of the models show a poleward shift of the zonal mean surface wind with a minimal increase in maximum strength (Supplementary Figure S5) and there is little agreement over the sign of change, apart from a decrease in westerly wind strength south of Australia and increase in strength over the Pacific sector (Figure 5c).

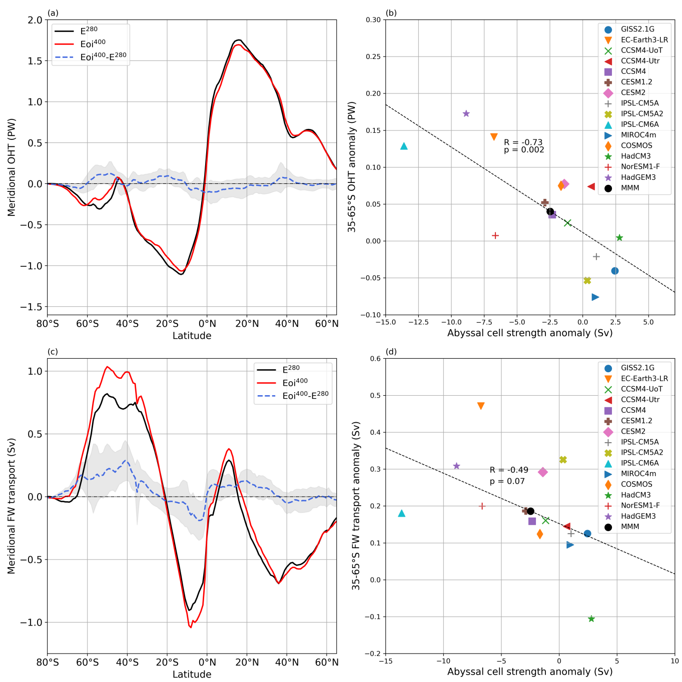

Figure 6. (a) MMM meridional ocean heat transport (OHT) in Eoi^{400}, E^{280} and Eoi^{400}–E^{280}, positive values indicate northward transport. Shading indicates one standard deviation around the MMM Eoi^{400}–E^{280} anomaly. (b) Scatter plot of the individual model Eoi^{400}–E^{280} abyssal cell strength anomaly against the 35°S-65°S-average global OHT anomaly. Dashed lines show a linear least-squares fit to the individual model data, with indicated correlation R- and p-values. (c), (d) Same as (a) and (b) for the meridional freshwater transport (FWT), respectively.

The Southern Ocean is the only location where the meridional ocean heat transport in the mid-Pliocene simulations differs significantly from the pre-industrial (Figure 6a, see Supplementary Figure S6 for individual model plots). Between 35°S–65°S, the MMM poleward heat transport reduces by 0.040 PW (-19%). We show in Figure 6b that the decrease in Southern Ocean OHT is significantly correlated with the decrease in abyssal cell strength ($R = -0.73$, $p = 0.002$). The 4 models that show an increase in poleward OHT in the Southern Ocean feature a stronger rather than weaker abyssal cell. These results suggest that mid-Pliocene changes in abyssal cell strength affect the Southern Ocean heat transport.

https://doi.org/10.5194/cp-2023-83
Preprint. Discussion started: 8 November 2023

In the Eoi^{400} simulations, we also find a significant increase in northward freshwater transport in the Southern Ocean with respect to the E^{280} (Figure 6c, see Supplementary Figure S7 for individual model plots). The northward freshwater transport increases between 35°S–65°S by 0.19 Sv (+31%). Figure 6d shows a correlation between the Southern Ocean freshwater transport anomaly and the abyssal cell strength that is just outside the 95% significance interval ($R = -0.49$, $p = 0.07$). The weakest increase or even decrease in northward freshwater transport is again shown by a subset of models that does not have a weaker abyssal cell circulation in the mid-Pliocene. It is also important to consider that the OHT and freshwater transport anomalies will likely be influenced by the stronger AMOC in the mid-Pliocene simulations. We do, however, not find a significant correlation between Southern Ocean heat or freshwater transport and the AMOC strength (Supplementary Figure S8).

2.3.2 Influence of boundary conditions and CO_2

The results in the previous section indicate that the density stratification of the mid-Pliocene Southern Ocean increases with respect to the pre-industrial in the PlioMIP2 ensemble, illustrating a significant impact on the global abyssal cell overturning circulation and its associated heat and freshwater transport. It is imperative to further investigate the cause for changes in temperature and salinity in the Southern Ocean that are driving increased density stratification in the mPWP. To this end, we employ the 7 available E^{400} sensitivity simulations to separate effects of CO_2 concentration and geographic boundary conditions, in particular the reduction of the Antarctic Ice Sheet in the Eoi^{400} simulations. In this section, for all the comparisons between Eoi^{400}, E^{400} and E^{280} cases we use the SMM, i.e. the mean of the 7 models that have an E^{400} simulation.

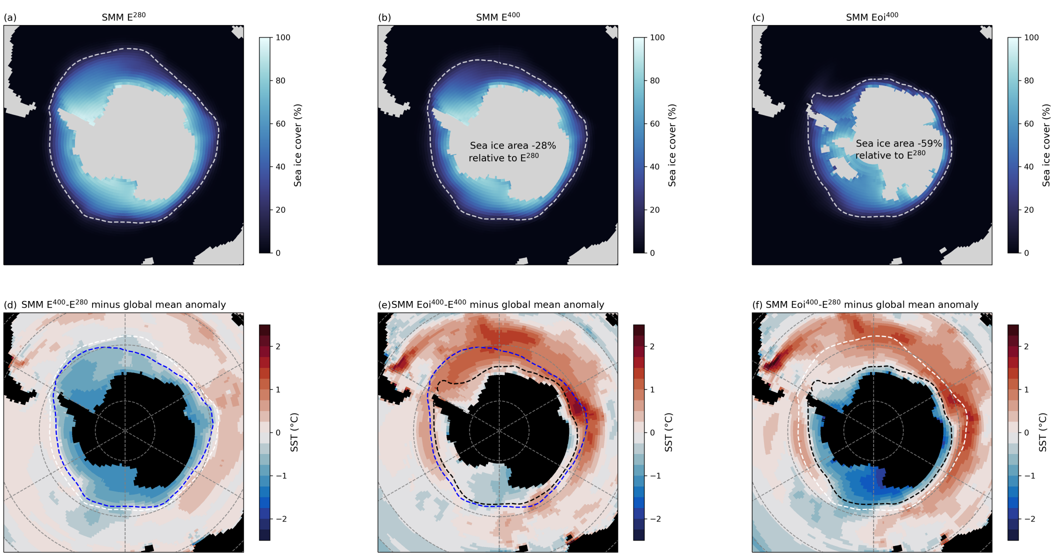

Figure 7. (a) SMM E^{280} sea-ice cover. White dashed line indicates the SMM sea-ice edge (15% sea-ice cover). (b),(c) Same as (a) for E^{400} and Eoi^{400}. (d) SMM E^{400}–E^{280} SST anomaly minus the MMM global mean SST anomaly. (e),(f) Same as (d) for Eoi^{400}–E^{400} and Eoi^{400}–E^{280}. White, blue and black dashed lines show the SMM sea-ice edge (15% sea-ice cover) in E^{280}, E^{400} and Eoi^{400}, respectively. Note that (f) is the same as Figure 1c but here the SMM is shown.

https://doi.org/10.5194/cp-2023-83
Preprint. Discussion started: 8 November 2023

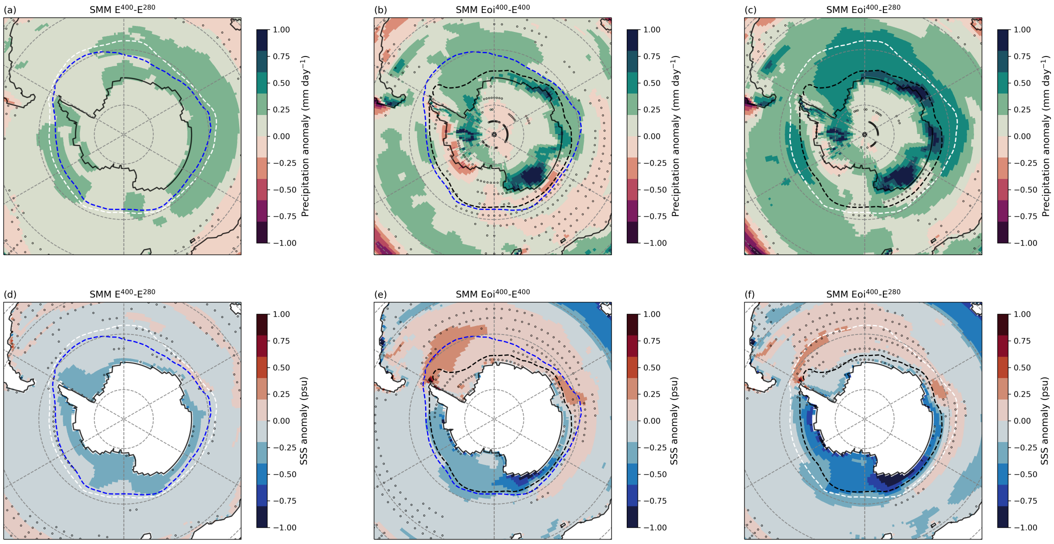

Figure 8. (a) SMM E^{400}–E^{280} precipitation anomaly. (b),(c) Same as (a) for Eoi^{400}–E^{400} and Eoi^{400}–E^{280}. White, blue and black dashed lines show the SMM sea-ice edge (15% sea-ice cover) in E^{280}, E^{400} and Eoi^{400}, respectively. Stippling indicates that less than 5 out of 7 (<70%) of the models included in the SMM agree on the sign of change. (d)-(f) Same as (a)-(c) but for sea surface salinity (SSS) anomaly.

Figure 7a-c illustrate that the effect of the mid-Pliocene boundary conditions on the sea-ice area is substantial. Where an increase in CO_2 from 280 ppm to 400 ppm causes a decrease in sea-ice area of 28% relative to the pre-industrial, implementing mid-Pliocene boundary conditions causes an additional 31% of sea-ice area loss. Figure 7d-f reinforces the earlier link that we found between enhanced warming in the Southern Ocean and sea-ice area decrease, in which we do not find an amplification of Southern Ocean warming in E^{400}. The SMM Southern Ocean SST amplification is 0.9 in E^{400} while the SMM Southern Ocean amplification index is 1.1 in Eoi^{400}, which is 0.1 lower than the MMM Eoi^{400} Southern Ocean amplification index. The Southern Ocean SST amplification observed in Eoi^{400} simulations is therefore mainly a consequence of the mPWP geographic boundary conditions. The SMM Southern Ocean average E^{400}–E^{280} SST anomaly is 1.1°C while the Eoi^{400}–E^{280} anomaly is 2.3°C. This means that the CO_2 forcing and mPWP boundary conditions both contribute approximately equally to mPWP Southern Ocean warming.

The SMM precipitation over the Southern Ocean and Antarctica is generally higher in Eoi^{400} than in E^{400} with respect to E^{280} (Figure 8a-c). Over the 45°S-90°S Southern Ocean, the average SMM precipitation increases by 0.18 mm day^{-1} (+7%) in E^{400} and 0.31 mm day^{-1} (+12%) in Eoi^{400}. The increase in precipitation over Antarctica is 0.10 mm day^{-1} in E^{400} (+14%) and 0.30 mm day^{-1} (+43%) in Eoi^{400}. The larger increase in precipitation over the Southern Ocean in Eoi^{400} results in a larger decrease in SMM sea surface salinity than in E^{400}, even though the mPWP boundary conditions also cause a substantial increase in evaporation over parts of the Southern Ocean and Antarctica (Supplementary Figure S9). On average, the sea surface salinity of the Southern Ocean decreases more in Eoi^{400} (-0.12 psu) than in E^{400} (-0.09 psu; Figure 8d-f). This difference is

https://doi.org/10.5194/cp-2023-83
Preprint. Discussion started: 8 November 2023

Climate of the Past Discussions

larger in the areas close to the Antarctic continent that are covered by sea-ice in Eoi^{400}. In these areas, the sea surface salinity decreases by 0.54 psu in Eoi^{400} and 0.24 psu in E^{400}.

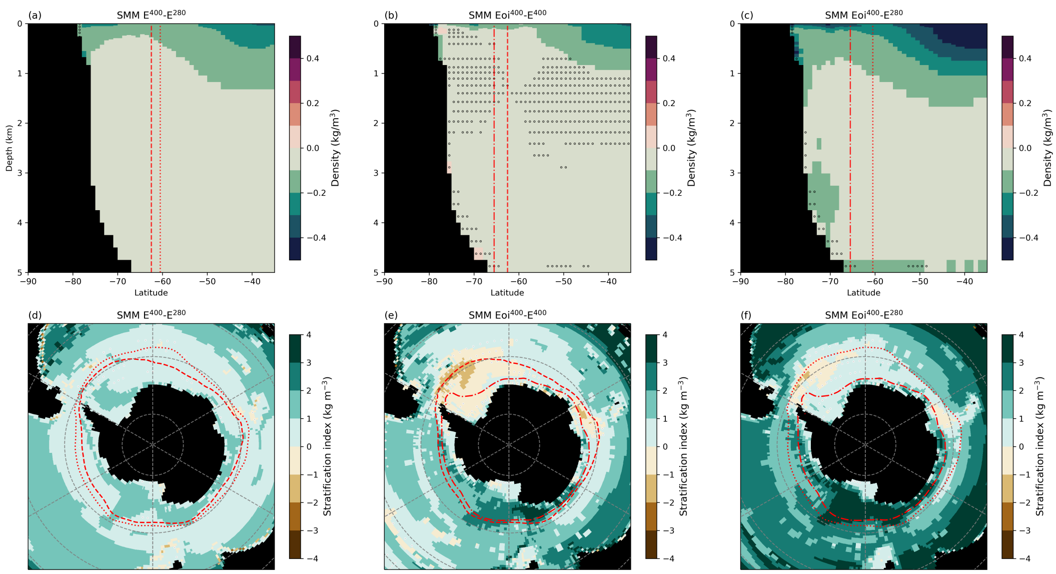

Figure 9. (a) Full-depth SMM zonal mean E^{400}–E^{280} potential density anomaly. (b),(c) Same as (a) for Eoi^{400}–E^{400} and Eoi^{400}–E^{280}. (d) SMM E^{400}–E^{280} stratification index anomaly. (e),(f) Same as (d) for Eoi^{400}–E^{400} and Eoi^{400}–E^{280}. Stippling indicates that less than 5 out of 7 (<70%) of the models included in the SMM agree on the sign of change. Red dotted, dashed and dashdotted lines show the SMM sea-ice edge (15% sea-ice cover) in E^{280}, E^{400} and Eoi^{400}, respectively.

In Figure 9a-c, we show the SMM zonal-mean potential density anomalies in the Southern Ocean. As expected, the warmer and fresher Southern Ocean surface in E^{400} also results in increased Southern Ocean stratification with respect to E^{280}. The SMM high-latitude (60°S-90°S) Southern Ocean stratification index increases by 0.7 kg m^{-3} in E^{400} (+14%) and 1.2 kg m^{-3} (+24%) in Eoi^{400} (Supplementary Table S1). Figure 9e shows that there are substantial regional variations in the SMM E^{400} and Eoi^{400} stratification indices. The Eoi^{400} SMM is less stratified in the Atlantic sector, possibly related to the stronger AMOC, while more stratified in the Indo-Pacific sector. At the mid-latitudes, the difference between SMM 45°S-60°S average Southern Ocean stratification index anomalies is larger: 0.8 kg m^{-3} in E^{400} (+10%) and 1.9 kg m^{-3} (+24%) in Eoi^{400}. These results suggest that across most of the Southern Ocean, mPWP boundary conditions enhance the increase in Southern Ocean stratification induced by a higher CO_2 level.

Despite the greater increase in stratification index in Eoi^{400} than in E^{400}, the abyssal cell shows a larger and more consistent decrease in the E^{400} simulations (Figure 10a). The SMM E^{400}–E^{280} abyssal cell strength anomaly, -1.9 Sv (-15%), is nearly double the Eoi^{400}–E^{280} anomaly of -1.0 Sv (+8%). There is a significant negative correlation between the stratification

https://doi.org/10.5194/cp-2023-83
Preprint. Discussion started: 8 November 2023

Climate of the Past Discussions

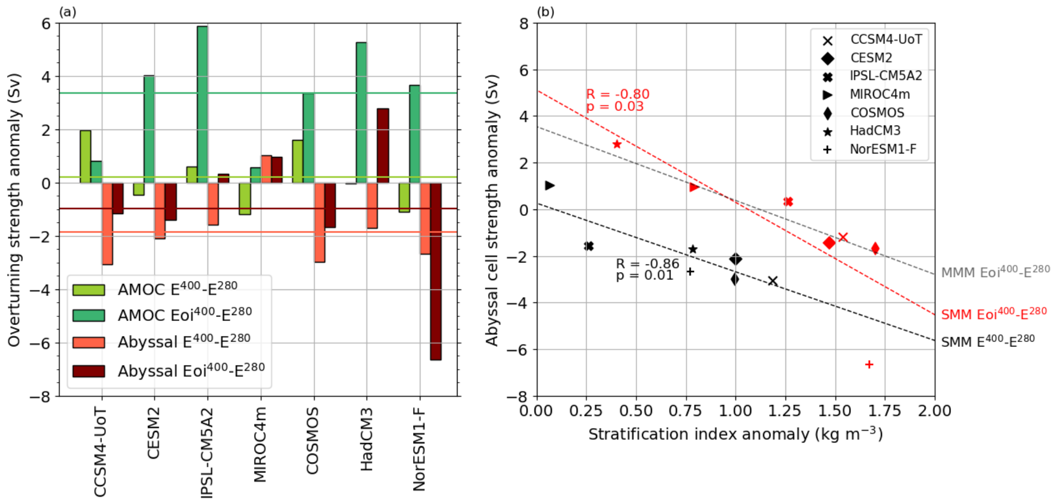

Figure 10. (a) SMM ensemble individual model Eoi^{400}–E^{280} and E^{400}–E^{280} AMOC (green) and abyssal overturning (red) strength anomalies. Horizontal lines indicate the SMM overturning strength anomalies. (b) Scatter plot of SMM ensemble individual model Eoi^{400}–E^{280} and E^{400}–E^{280} Southern Ocean stratification index anomalies against the abyssal cell strength anomalies. Dashed lines show a linear least-squares fit to the individual model data, with indicated correlation R- and p-values. The MMM regression from Figure 4b is shown in light grey.

index anomaly and the abyssal cell strength anomaly for both E^{400}–E^{280} and Eoi^{400}–E^{280}, as shown in Figure 10b. The difference between the slope and y-intercept of the E^{400}–E^{280} and Eoi^{400}–E^{280} regressions is likely to be related to the interaction of the abyssal circulation with the AMOC. The results suggest that the stronger AMOC in Eoi^{400} may be partly compensating weakening of the abyssal cell. The AMOC cell is stronger in all Eoi^{400} simulations with respect to E^{280} (Figure 10a), with an SMM increase of 3.4 Sv (+18%), while the E^{400} SMM AMOC strength increase of 0.2 (+1%) is substantially lower, and only 3 out of 7 models simulate a stronger AMOC in E^{400}.

2.4 Discussion

2.4.1 Mid-Pliocene Southern Ocean as a future analog

Burton et al. (2023) have shown that the influence of mPWP boundary conditions on the simulated global average mPWP–PI SAT, SST, and precipitation anomalies in PlioMIP2 is substantial. They find that 44% of the SAT and SST anomaly and 49% of the precipitation anomaly were driven by non-CO_2 forcing. Our results align with this study and show that the mPWP boundary conditions are responsible for approximately half of the average mPWP–PI anomaly in sea-ice cover, SST, precipitation and stratification index in the Southern Ocean. While a separation of effects due to orographic and land ice cover is not possible, it is plausible that this influence is primarily due to the decreased Antarctic Ice Sheet as there are, apart from a closed Indonesian Throughflow, little other changes in SH mPWP boundary conditions with respect to the PI. This may make the mid-Pliocene

https://doi.org/10.5194/cp-2023-83
Preprint. Discussion started: 8 November 2023

Climate of the Past Discussions

warm period a good analog for our long-term future climate, in which substantial melt of the Antarctic Ice Sheet is expected. We show that mPWP boundary conditions, primarily the reduction of the Antarctic Ice Sheet in the Southern Hemisphere, lead to additional precipitation, sea-ice loss and sea surface warming, and are thus responsible for reinforcing increased stratification caused by a rise in CO_2 levels. This potential effect of Antarctic Ice Sheet reduction is not taken into account in the CMIP projection of future climate, but may therefore play an important role in Southern Ocean conditions on multi-centennial time scales. Moreover, a slowly changing ice sheet will contribute to changes in equilibrium climate sensitivity due to state dependence of fast feedback processes (von der Heydt et al., 2016), which is not accounted for in CMIP simulations and multi-century ice sheet projections. It should be taken into account, however, that Antarctic Ice Sheet projections do not show a ~ 24 m sea level equivalent decrease in ice volume. Under unabated emission scenario's, multi-centennial projections show a maximum increase in sea-level equivalent melt between approximately 5 m (Golledge et al., 2015) and 15 m (DeConto and Pollard, 2016) by 2500 CE, which makes the mPWP ice sheet extent unrealistic even for longer-term future scenario's. This means that the Southern Ocean conditions from this study are not likely to be analogous to a long-term future, although a partial reduction, that includes the collapse of the West Antarctic Ice Sheet, would still greatly decrease the ice sheet extent and therefore possibly induce effects similar to those found in this study.

Our results suggest a relationship between increased stratification in the Southern Ocean and a weakened abyssal cell circulation during the mid-Pliocene warm period. CMIP5 studies also show a decline in Antarctic Bottom Water formation due to fresher and warmer Southern Ocean surface conditions, and consequentially a slowdown of deep ocean circulation (Meijers, 2014; Ito et al., 2015). There are six out of fifteen ensemble members that demonstrate an increase in Southern Ocean stratification in the mPWP simulations without weaker abyssal cell circulation. Interestingly, four of these six models also exhibit the largest AMOC strength increase during the mPWP with respect to the PI. This implies a potential linkage between the AMOC and abyssal cell circulation where a stronger AMOC during the mid-Pliocene may partially compensate for the reduced formation and circulation of Southern Ocean bottom water. The stronger AMOC in the mPWP PlioMIP2 simulations has been attributed to changes in geographical boundary conditions, specifically the closure of the Bering Strait and Canadian Archipelago (Weiffenbach et al., 2023). Consequently, a question arises regarding the extent to which the decline in abyssal cell circulation, or the lack of decline exhibited in some models, resembles a plausible future scenario. Given the substantial influence of the intensified AMOC in the mPWP PlioMIP2 simulations on global ocean circulation, it is reasonable to expect it also impacts Southern Ocean conditions. To disentangle effects of orographic and ice sheet changes, additional sensitivity studies are necessary. Nevertheless, our results highlight the tight interplay between AMOC and abyssal cell, connecting Southern and Northern Hemisphere high latitudes as well as their potential to impact fast feedback processes relevant for equilibrium climate sensitivity in various regions of the world.

2.4.2 Model-data comparison

There is no data on the Southern Ocean sea-ice cover during the KM5c time slice, but there are a number of studies on Pliocene sea-ice and ocean temperatures that suggest there was reduced ice cover during this period (e.g., Barron, 1996; Whitehead

https://doi.org/10.5194/cp-2023-83
Preprint. Discussion started: 8 November 2023

and Bohaty, 2003; Whitehead et al., 2005; Dowsett et al., 2010). Whitehead et al. (2005) reconstruct winter sea-ice at Site 1165 (64.380°S, 67.219°E and Site 1166 (67.696°S, 74.787°E) across the Pliocene. They find a maximum of 78% less sea-ice relative to modern at Site 1165, and a 61% reduction at Site 1166 during the Pliocene. Our MMM shows a respective relative sea-ice concentration decrease of 72% and 39% at these locations, respectively, which matches reconstructions reasonably well considering the range of uncertainty in the reconstructions of at least 30% (Whitehead et al., 2005).

We also compare Southern Ocean PlioMIP2 SSTs to SST reconstructions from the KM5c time slice. The SST reconstruction by McClymont et al. (2020) includes 6 proxy locations in (close proximity to) the Southern Ocean. We compare absolute mPWP SSTs and mPWP–PI SST anomalies at these locations for both the models and data in Supplementary Figure S10, using the SSTs from the ERSSTv5 1870-1900 dataset (Huang et al. (2017) as the pre-industrial observations and reconstructions by McClymont et al. (2020) as observed mPWP SSTs. While absolute mPWP SST reconstructions generally fall within the range of the PlioMIP2 ensemble SSTs, the average spread of modelled mPWP SSTs is 7.9°C. This intermodel spread is reduced to 4.1°C for the mPWP–PI SST anomalies. However, at three out of six SST proxy locations, the reconstructed SST anomaly falls outside the range of the modelled SST anomaly. The models are neither consistently warmer nor colder than the reconstructions, meaning we cannot detect a consistent bias in the modelled or reconstructed Southern Ocean SSTs. The models appear to match absolute mPWP Southern Ocean SSTs reconstructions better than reconstructed mPWP–PI SST anomalies, possibly due discrepancies between reconstructed and modelled Southern Ocean SSTs in the PI.

2.4.3 Southern Ocean biases

From historical CMIP5 and CMIP6 simulations, it is known that low-resolution earth system models show systematic biases and inaccuracies concerning Southern Ocean surface conditions and deep ocean circulation. Southern Ocean SSTs are among the most (warm) biased characteristics of Earth System model simulations (e.g. Wang et al., 2022; Zhang et al., 2023)). CMIP5 simulations have been shown to have a consistent warm and low-density bias over the entire water column and show a large spread in the volume and characteristics of Antarctic bottom water (Sallée et al., 2013). As most CMIP5 models create deep water by deep convection in the open ocean, which only rarely occurs in reality, bottom water formation processes are not well represented in these low-resolution GCMs (Heuzé et al., 2013). This remains a problem in the newer CMIP6 generation models (Mohrmann et al., 2021). The majority of the PlioMIP2 models are models also used for CMIP5 or CMIP6, and therefore have the same issues representing deep water formation. As such, changes to deep cell circulation in the mid-Pliocene warm period may also be biased due the inaccurate representation of deep water formation in the Southern Ocean. In addition, it has been shown that the CMIP5 ensemble shows biases in Southern Ocean SSTs due to errors in cloud-related parametrizations (Hyder et al., 2018). These biases have been correlated to simulated Last Glacial Maximum AMOC depth anomalies (Sherriff-Tadano et al., 2023) and could potentially also affect the AMOC and deep cell circulation in the mPWP.

Another important bias in the PlioMIP2 models concerns the sea-ice area. It has been shown that changes in temperature,

https://doi.org/10.5194/cp-2023-83
Preprint. Discussion started: 8 November 2023

sea-ice area and precipitation in future projections are strongly tied to the simulated historical mean sea-ice area in CMIP5 (Bracegirdle et al., 2015; Kajtar et al., 2021) and the models strongly overestimate the historical variance of sea-ice extent (Zunz et al., 2013). The PlioMIP2 ensemble also features large ranges of uncertainty in sea-ice cover, which we have shown to be crucial when it comes to polar amplification and Southern Ocean precipitation. Supplementary Figure S11 shows that MMM sea-ice cover and extent in the PI E^{280} simulations roughly matches historical observations (1979-2004 NOAA/NSIDC Climate Data Record of Passive Microwave Sea Ice Concentration, Meier, W.N. et al. (2021)), with a MMM E^{280} sea-ice area of 10.4 million km^2 and present-day observed sea-ice area of 9.5 million km^2. However, the sea-ice area variation among models is 5.2-15.6 million km^2, which is substantially larger than the discrepancy between the MMM E^{280} and present-day observations. Furthermore, the absolute Eoi^{400}–E^{280} sea-ice area anomaly varies between -4.0 and -11.7 million km^2, and relative sea-ice area anomaly between -39% and -96%. This large variance in sea-ice extent leads to uncertainty about the representativeness of the Southern Ocean conditions in response to both the higher CO_2 and the geographic boundary conditions in the mPWP, especially for those models that have a substantially lower or higher sea-ice cover than the MMM.

3 Conclusions

The Southern Ocean simulated by PlioMIP2 is characterized by a large reduction in sea-ice area in the mid-Pliocene warm period with respect to the pre-industrial. Due to the increase of CO_2 and Antarctic Ice Sheet reduction, the 60°S-90°S MMM SAT is 7.6°C warmer in the mPWP. This results in a polar amplification factor of 2.2 with respect to the global average MMM SAT of 3.4°C, which is substantially higher than in future projections. The MMM relative sea-ice area decrease is 71%, with a substantial variation in sea-ice area decrease among the 15 models that ranges from -39% to -96%. The decrease in Southern Ocean sea-ice area is strongly tied to the SST increase in the mPWP, ranging from 1.1°C to 5.1°C with a MMM increase of 2.8°C. There is also a robust increase in precipitation, with a MMM increase of 0.35 mm per day over the mPWP Southern Ocean and Antarctic continent, resulting in freshening of the ocean surface.

The warm and fresh mPWP Southern Ocean surface leads to an increase in density stratification with respect to the pre-industrial. This is correlated with a slowdown of the global abyssal cell circulation during the mid-Pliocene warm period, affecting both heat and freshwater transport in the Southern Ocean. The CO_2 concentration and Antarctic Ice Sheet reduction are primary drivers of warmer and fresher Southern Ocean surface conditions and of deep ocean circulation in the mid-Pliocene warm period with respect to the pre-industrial. However, we do find a potential interaction of deep abyssal circulation with the stronger AMOC in the mPWP simulations, where the strengthened AMOC partly compensates weakening of the abyssal cell. Increased AMOC strength has been linked to high North Atlantic salinity due to closed Arctic gateways during the mid-Pliocene warm period and therefore does not appear to be directly related to the CO_2 increase or Antarctic Ice Sheet reduction.

Sensitivity simulations at the mid-Pliocene CO_2 level without any geographic, ice sheet or vegetation changes also show decreased sea-ice area, increased precipitation, and warming and freshening of the ocean surface. This effect is enhanced by mid-Pliocene boundary conditions, in particular by the Antarctic Ice Sheet reduction, where these boundary conditions contribute approximately one half to the total sea-ice area loss, SST warming, precipitation increase and density stratification increase in the mPWP simulations. This illustrates that it is important to consider the effects of a smaller Antarctic Ice Sheet when projecting for possible long-term future climates. The multi-century reduction of the Antarctic ice sheet will drive changes in fast feedback processes (e.g. clouds, sea-ice cover) affecting equilibrium climate sensitivity. However, uncertainties are present via the large model spread and biases in sea-ice area and Southern Ocean deep water formation, as well as via the effect of orographic changes on ocean circulation and Southern Ocean conditions. Additional sensitivity studies, where land-sea mask and ice sheet size are implemented separately, are necessary to be able to separate the effect of orography and ice sheet changes in the mPWP simulations and further investigate the mechanisms behind the mid-Pliocene Southern Ocean's effect on global ocean circulation.

Data availability. PlioMIP2 data used for this paper is available upon request from Alan M. Haywood (a.m.haywood@leeds.ac.uk), with the exception of IPSL-CM6A, EC-Earth3-LR and GISS2.1G. PlioMIP2 data from IPSL-CM6A, EC-Earth3-LR and GISS2.1G can be obtained from the Earth System Grid Federation (ESGF) (https://esgf-node.llnl.gov/search/cmip6/, last access: 10 March 2023). The $U_{37}^{k'}$ and Mg/Ca SST reconstructions from McClymont et al. (2020) can be obtained through https://doi.pangaea.de/10.1594/PANGAEA.911847 (last access: 24 January 2022). The NOAA/NSIDC Climate Data Record of Passive Microwave Sea Ice Concentration dataset from Meier, W.N. et al. (2021) can be obtained through https://doi.org/10.7265/efmz-2t65 (last access: 23 June 2023). The observational pre-industrial SSTs from the NOAA ERSST5 dataset (Huang et al., 2017) can be downloaded from https://www.ncei.noaa.gov/products/extended-reconstructed-sst (last access: 24 January 2022).

Author contributions. JEW, HAD and ASvdH designed the work. JEW performed the analysis and wrote the manuscript of the paper with contributions from all the co-authors. AAO, WLC, DC, RF, AMH, SJH, XL, BLOB, WRP, CS, NT, JCT and ZZ provided data from the PlioMIP2 experiments.

Competing interests. At least one of the (co-)authors is a member of the editorial board of *Climate of the Past*.

Acknowledgements. The work by Julia E. Weiffenbach, Henk A. Dijkstra and Anna S. von der Heydt was carried out under the program of the Netherlands Earth System Science Centre (NESSC), financially supported by the Ministry of Education, Culture and Science (OCW grant number 024.002.001). CCSM4-Utr simulations were performed at the SURFsara Dutch national computing facilities and were sponsored by NWO-EW (Netherlands Organisation for Scientific Research, Exact Sciences) under the projects 17189 and 2020.022.

Ayako Abe-Ouchi and Wing-Le Chan acknowledge funding from JSPS KAKENHI (grant no. 17H06104) and MEXT KAKENHI (grant no. 17H06323) and are grateful to JAMSTEC for use of the Earth Simulator.

Deepak Chandan and W. Richard Peltier were supported by Canadian NSERC Discovery Grant A9627, and they wish to acknowledge the support of the SciNet HPC Consortium for providing computing facilities. SciNet is funded by the Canada Foundation for Innovation under the auspices of Compute Canada, the Government of Ontario, the Ontario Research Fund – Research Excellence and the University of Toronto.

Ran Feng acknowledges support from the US National Science Foundation grant numbers NSF-2103055 and NSF-2238875. The CCSM4 and CESM1 and CESM2 simulations are performed with high-performance computing support from Cheyenne (https://doi.org/10.5065/D6RX99HX) provided by NCAR's Computational and Information Systems Laboratory, sponsored by the National Science Foundation.

Alan M. Haywood, Stephen J. Hunter and Julia C. Tindall acknowledge the FP7 Ideas program from the European Research Council (grant no. PLIO-ESS, 278636), the Past Earth Network (EPSRC grant no. EP/M008.363/1) and the University of Leeds Advanced Research Computing service. Julia C. Tindall was also supported through the Centre for Environmental Modelling and Computation (CEMAC), University of Leeds.

Christian Stepanek acknowledges funding from the Helmholtz Climate Initiative REKLIM and the research program PACES-II of the Helmholtz Association.

Ning Tan was granted access to the HPC resources of TGCC under the allocations 2016A0030107732, 2017-R0040110492 and 2018-R0040110492 (gencmip6) as well as 2019-A0050102212 (gen2212) provided by GENCI.

Zhongshi Zhang and Xiangyu Li acknowledge financial support from the National Natural Science Foundation of China (grant no. 42005042), the China Scholarship Council (201804910023) and the China Postdoctoral Science Foundation (project no. 2015M581154). The NorESM simulations benefitted from resources provided by UNINETT Sigma2 – the National Infrastructure for High Performance Computing and Data Storage in Norway.

https://doi.org/10.5194/cp-2023-83
Preprint. Discussion started: 8 November 2023

References

Almeida, L., Mazloff, M. R., and Mata, M. M.: The Impact of Southern Ocean Ekman Pumping, Heat and Freshwater Flux Variability on Intermediate and Mode Water Export in CMIP Models: Present and Future Scenarios, Journal of Geophysical Research: Oceans, 126, e2021JC017 173, https://doi.org/10.1029/2021JC017173, 2021.

Baatsen, M. L. J., von der Heydt, A. S., Kliphuis, M. A., Oldeman, A. M., and Weiffenbach, J. E.: Warm mid-Pliocene conditions without high climate sensitivity: the CCSM4-Utrecht (CESM 1.0.5) contribution to the PlioMIP2, Climate of the Past, https://doi.org/10.5194/cp-2021-140, 2022.

Barron, J. A.: Diatom constraints on the position of the Antarctic Polar Front in the middle part of the Pliocene, Marine Micropaleontology, 27, 195–213, https://doi.org/10.1016/0377-8398(95)00060-7, 1996.

Bopp, L., Lévy, M., Resplandy, L., and Sallée, J. B.: Pathways of anthropogenic carbon subduction in the global ocean, Geophysical Research Letters, 42, 6416–6423, https://doi.org/10.1002/2015GL065073, 2015.

Bourgeois, T., Goris, N., Schwinger, J., and Tjiputra, J. F.: Stratification constrains future heat and carbon uptake in the Southern Ocean between 30°S and 55°S, Nature Communications, 13, 340, https://doi.org/10.1038/s41467-022-27979-5, 2022.

Bracegirdle, T. J., Shuckburgh, E., Sallee, J.-B., Wang, Z., Meijers, A. J. S., Bruneau, N., Phillips, T., and Wilcox, L. J.: Assessment of surface winds over the Atlantic, Indian, and Pacific Ocean sectors of the Southern Ocean in CMIP5 models: historical bias, forcing response, and state dependence, Journal of Geophysical Research: Atmospheres, 118, 547–562, https://doi.org/10.1002/jgrd.50153, 2013.

Bracegirdle, T. J., Stephenson, D. B., Turner, J., and Phillips, T.: The importance of sea ice area biases in 21st century multimodel projections of Antarctic temperature and precipitation, Geophysical Research Letters, 42, 10,832–10,839, https://doi.org/10.1002/2015GL067055, 2015.

Bracegirdle, T. J., Krinner, G., Tonelli, M., Haumann, F. A., Naughten, K. A., Rackow, T., Roach, L. A., and Wainer, I.: Twenty first century changes in Antarctic and Southern Ocean surface climate in CMIP6, Atmospheric Science Letters, 21, e984, https://doi.org/10.1002/asl.984, 2020.

Bulthuis, K., Arnst, M., Sun, S., and Pattyn, F.: Uncertainty quantification of the multi-centennial response of the Antarctic ice sheet to climate change, The Cryosphere, 13, 1349–1380, https://doi.org/10.5194/tc-13-1349-2019, 2019.

Burke, K. D., Williams, J. W., Chandler, M. A., Haywood, A. M., Lunt, D. J., and Otto-Bliesner, B. L.: Pliocene and Eocene provide best analogs for near-future climates, Proceedings of the National Academy of Sciences, 115, 13 288–13 293, https://doi.org/10.1073/pnas.1809600115, 2018.

Burton, L. E., Haywood, A. M., Tindall, J. C., Dolan, A. M., Hill, D. J., Abe-Ouchi, A., Chan, W.-L., Chandan, D., Feng, R., Hunter, S. J., Li, X., Peltier, W. R., Tan, N., Stepanek, C., and Zhang, Z.: On the climatic influence of CO2 forcing in the Pliocene, Climate of the Past, 19, 747–764, https://doi.org/10.5194/cp-19-747-2023, 2023.

Chan, W.-L. and Abe-Ouchi, A.: Pliocene Model Intercomparison Project (PlioMIP2) simulations using the Model for Interdisciplinary Research on Climate (MIROC4m), Climate of the Past, 16, 1523–1545, https://doi.org/10.5194/cp-16-1523-2020, 2020.

Chandan, D. and Peltier, W. R.: Regional and global climate for the mid-Pliocene using the University of Toronto version of CCSM4 and PlioMIP2 boundary conditions, Climate of the Past, 13, 919–942, https://doi.org/10.5194/cp-13-919-2017, 2017.

Cornford, S. L., Martin, D. F., Payne, A. J., Ng, E. G., Le Brocq, A. M., Gladstone, R. M., Edwards, T. L., Shannon, S. R., Agosta, C., van den Broeke, M. R., Hellmer, H. H., Krinner, G., Ligtenberg, S. R. M., Timmermann, R., and Vaughan, D. G.: Century-scale simulations of the

https://doi.org/10.5194/cp-2023-83
Preprint. Discussion started: 8 November 2023

Climate of the Past
Discussions

response of the West Antarctic Ice Sheet to a warming climate, The Cryosphere, 9, 1579–1600, https://doi.org/10.5194/tc-9-1579-2015, 2015.

de la Vega, E., Chalk, T. B., Wilson, P. A., Bysani, R. P., and Foster, G. L.: Atmospheric CO2 during the Mid-Piacenzian Warm Period and the M2 glaciation, Scientific Reports, 10, 11 002, https://doi.org/10.1038/s41598-020-67154-8, 2020.

DeConto, R. M. and Pollard, D.: Contribution of Antarctica to past and future sea-level rise, Nature, 531, 591–597, https://doi.org/10.1038/nature17145, 2016.

Deng, K., Azorin-Molina, C., Yang, S., Hu, C., Zhang, G., Minola, L., and Chen, D.: Changes of Southern Hemisphere westerlies in the future warming climate, Atmospheric Research, 270, 106 040, https://doi.org/10.1016/j.atmosres.2022.106040, 2022.

Dolan, A. M., Hunter, S. J., Hill, D. J., Haywood, A. M., Koenig, S. J., Otto-Bliesner, B. L., Abe-Ouchi, A., Bragg, F., Chan, W.-L., Chandler, M. A., Contoux, C., Jost, A., Kamae, Y., Lohmann, G., Lunt, D. J., Ramstein, G., Rosenbloom, N. A., Sohl, L., Stepanek, C., Ueda, H., Yan, Q., and Zhang, Z.: Using results from the PlioMIP ensemble to investigate the Greenland Ice Sheet during the mid-Pliocene Warm Period, Climate of the Past, 11, 403–424, https://doi.org/10.5194/cp-11-403-2015, 2015.

Dowsett, H., Robinson, M., Haywood, A., Salzmann, U., Hill, D., Sohl, L., Chandler, M., Williams, M., Foley, K., and Stoll, D.: The PRISM3D paleoenvironmental reconstruction, Stratigraphy, 7, 17, http://pubs.er.usgs.gov/publication/70044350, 2010.

Dowsett, H., Dolan, A., Rowley, D., Moucha, R., Forte, A. M., Mitrovica, J. X., Pound, M., Salzmann, U., Robinson, M., Chandler, M., Foley, K., and Haywood, A.: The PRISM4 (mid-Piacenzian) paleoenvironmental reconstruction, Climate of the Past, 12, 1519–1538, https://doi.org/10.5194/cp-12-1519-2016, 2016.

Eyring, V., Bony, S., Meehl, G. A., Senior, C. A., Stevens, B., Stouffer, R. J., and Taylor, K. E.: Overview of the Coupled Model Intercomparison Project Phase 6 (CMIP6) experimental design and organization, Geoscientific Model Development, 9, 1937–1958, https://doi.org/10.5194/gmd-9-1937-2016, 2016.

Feng, R., Otto-Bliesner, B. L., Brady, E. C., and Rosenbloom, N.: Increased Climate Response and Earth System Sensitivity From CCSM4 to CESM2 in Mid-Pliocene Simulations, Journal of Advances in Modeling Earth Systems, 12, https://doi.org/10.1029/2019MS002033, 2020.

Feng, R., Bhattacharya, T., Otto-Bliesner, B. L., Brady, E. C., Haywood, A. M., Tindall, J. C., Hunter, S. J., Abe-Ouchi, A., Chan, W.-L., Kageyama, M., Contoux, C., Guo, C., Li, X., Lohmann, G., Stepanek, C., Tan, N., Zhang, Q., Zhang, Z., Han, Z., Williams, C. J. R., Lunt, D. J., Dowsett, H. J., Chandan, D., and Peltier, W. R.: Past terrestrial hydroclimate sensitivity controlled by Earth system feedbacks, Nature Communications, 13, 1306, https://doi.org/10.1038/s41467-022-28814-7, 2022.

Frölicher, T. L., Sarmiento, J. L., Paynter, D. J., Dunne, J. P., Krasting, J. P., and Winton, M.: Dominance of the Southern Ocean in Anthropogenic Carbon and Heat Uptake in CMIP5 Models, Journal of Climate, 28, 862–886, https://doi.org/10.1175/JCLI-D-14-00117.1, 2015.

Golledge, N. R., Kowalewski, D. E., Naish, T. R., Levy, R. H., Fogwill, C. J., and Gasson, E. G. W.: The multi-millennial Antarctic commitment to future sea-level rise, Nature, 526, 421–425, https://doi.org/10.1038/nature15706, 2015.

Hahn, L. C., Armour, K. C., Zelinka, M. D., Bitz, C. M., and Donohoe, A.: Contributions to Polar Amplification in CMIP5 and CMIP6 Models, Frontiers in Earth Science, 9, https://www.frontiersin.org/articles/10.3389/feart.2021.710036, 2021.

Haywood, A., Dowsett, H., Dolan, A., Rowley, D., Abe-Ouchi, A., Otto-Bliesner, B., Chandler, M., Hunter, S., Lunt, D., Pound, M., and Salzmann, U.: The Pliocene Model Intercomparison Project (PlioMIP) Phase 2: scientific objectives and experimental design, Climate of the Past, 12, 663–675, https://doi.org/10.5194/cp-12-663-2016, 2016.

https://doi.org/10.5194/cp-2023-83
Preprint. Discussion started: 8 November 2023

Haywood, A. M., Hill, D. J., Dolan, A. M., Otto-Bliesner, B. L., Bragg, F., Chan, W.-L., Chandler, M. A., Contoux, C., Dowsett, H. J., Jost, A., Kamae, Y., Lohmann, G., Lunt, D. J., Abe-Ouchi, A., Pickering, S. J., Ramstein, G., Rosenbloom, N. A., Salzmann, U., Sohl, L., Stepanek, C., Ueda, H., Yan, Q., and Zhang, Z.: Large-scale features of Pliocene climate: results from the Pliocene Model Intercomparison Project, Climate of the Past, 9, 191–209, https://doi.org/10.5194/cp-9-191-2013, 2013.

Haywood, A. M., Tindall, J. C., Dowsett, H. J., Dolan, A. M., Foley, K. M., Hunter, S. J., Hill, D. J., Chan, W.-L., Abe-Ouchi, A., Stepanek, C., Lohmann, G., Chandan, D., Peltier, W. R., Tan, N., Contoux, C., Ramstein, G., Li, X., Zhang, Z., Guo, C., Nisancioglu, K. H., Zhang, Q., Li, Q., Kamae, Y., Chandler, M. A., Sohl, L. E., Otto-Bliesner, B. L., Feng, R., Brady, E. C., von der Heydt, A. S., Baatsen, M. L. J., and Lunt, D. J.: The Pliocene Model Intercomparison Project Phase 2: large-scale climate features and climate sensitivity, Climate of the Past, 16, 2095–2123, https://doi.org/10.5194/cp-16-2095-2020, 2020.

Heuzé, C., Heywood, K. J., Stevens, D. P., and Ridley, J. K.: Southern Ocean bottom water characteristics in CMIP5 models, Geophysical Research Letters, 40, 1409–1414, https://doi.org/10.1002/grl.50287, 2013.

Huang, B., Thorne, P. W., Banzon, V. F., Boyer, T., Chepurin, G., Lawrimore, J. H., Menne, M. J., Smith, T. M., Vose, R. S., and Zhang, H.-M.: Extended Reconstructed Sea Surface Temperature, Version 5 (ERSSTv5): Upgrades, Validations, and Intercomparisons, Journal of Climate, 30, 8179–8205, https://doi.org/10.1175/JCLI-D-16-0836.1, 2017.

Hunter, S. J., Haywood, A. M., Dolan, A. M., and Tindall, J. C.: The HadCM3 contribution to PlioMIP phase 2, Climate of the Past, 15, 1691–1713, https://doi.org/10.5194/cp-15-1691-2019, 2019.

Hyder, P., Edwards, J. M., Allan, R. P., Hewitt, H. T., Bracegirdle, T. J., Gregory, J. M., Wood, R. A., Meijers, A. J. S., Mulcahy, J., Field, P., Furtado, K., Bodas-Salcedo, A., Williams, K. D., Copsey, D., Josey, S. A., Liu, C., Roberts, C. D., Sanchez, C., Ridley, J., Thorpe, L., Hardiman, S. C., Mayer, M., Berry, D. I., and Belcher, S. E.: Critical Southern Ocean climate model biases traced to atmospheric model cloud errors, Nature Communications, 9, 3625, https://doi.org/10.1038/s41467-018-05634-2, 2018.

Ito, T., Bracco, A., Deutsch, C., Frenzel, H., Long, M., and Takano, Y.: Sustained growth of the Southern Ocean carbon storage in a warming climate, Geophysical Research Letters, 42, 4516–4522, https://doi.org/10.1002/2015GL064320, 2015.

Iudicone, D., Rodgers, K. B., Stendardo, I., Aumont, O., Madec, G., Bopp, L., Mangoni, O., and Ribera d'Alcala', M.: Water masses as a unifying framework for understanding the Southern Ocean Carbon Cycle, Biogeosciences, 8, 1031–1052, https://doi.org/10.5194/bg-8-1031-2011, 2011.

Johnson, G. C.: Quantifying Antarctic Bottom Water and North Atlantic Deep Water volumes, Journal of Geophysical Research: Oceans, 113, https://doi.org/10.1029/2007JC004477, 2008.

Kajtar, J. B., Santoso, A., Collins, M., Taschetto, A. S., England, M. H., and Frankcombe, L. M.: CMIP5 Intermodel Relationships in the Baseline Southern Ocean Climate System and With Future Projections, Earth's Future, 9, e2020EF001 873, https://doi.org/10.1029/2020EF001873, 2021.

Khatiwala, S., Primeau, F., and Hall, T.: Reconstruction of the history of anthropogenic CO2 concentrations in the ocean, Nature, 462, 346–349, https://doi.org/10.1038/nature08526, 2009.

Kidston, J. and Gerber, E. P.: Intermodel variability of the poleward shift of the austral jet stream in the CMIP3 integrations linked to biases in 20th century climatology, Geophysical Research Letters, 37, https://doi.org/10.1029/2010GL042873, 2010.

Li, X., Guo, C., Zhang, Z., Otterå, O. H., and Zhang, R.: PlioMIP2 simulations with NorESM-L and NorESM1-F, Climate of the Past, 16, 183–197, https://doi.org/10.5194/cp-16-183-2020, 2020.

Liu, W., Lu, J., Xie, S.-P., and Fedorov, A.: Southern Ocean Heat Uptake, Redistribution, and Storage in a Warming Climate: The Role of Meridional Overturning Circulation, Journal of Climate, 31, 4727–4743, https://doi.org/10.1175/JCLI-D-17-0761.1, 2018.

https://doi.org/10.5194/cp-2023-83
Preprint. Discussion started: 8 November 2023

Lumpkin, R. and Speer, K.: Global Ocean Meridional Overturning, Journal of Physical Oceanography, 37, 2550–2562, https://doi.org/10.1175/JPO3130.1, 2007.

Lurton, T., Balkanski, Y., Bastrikov, V., Bekki, S., Bopp, L., Braconnot, P., Brockmann, P., Cadule, P., Contoux, C., Cozic, A., Cugnet, D., Dufresne, J., Éthé, C., Foujols, M., Ghattas, J., Hauglustaine, D., Hu, R., Kageyama, M., Khodri, M., Lebas, N., Levavasseur, G., Marchand, M., Ottlé, C., Peylin, P., Sima, A., Szopa, S., Thiéblemont, R., Vuichard, N., and Boucher, O.: Implementation of the CMIP6 Forcing Data in the IPSL-CM6A-LR Model, Journal of Advances in Modeling Earth Systems, 12, https://doi.org/10.1029/2019MS001940, 2020.

Marshall, J. and Speer, K.: Closure of the meridional overturning circulation through Southern Ocean upwelling, Nature Geoscience, 5, 171–180, https://doi.org/10.1038/ngeo1391, 2012.

McClymont, E. L., Ford, H. L., Ho, S. L., Tindall, J. C., Haywood, A. M., Alonso-Garcia, M., Bailey, I., Berke, M. A., Littler, K., Patterson, M. O., Petrick, B., Peterse, F., Ravelo, A. C., Risebrobakken, B., De Schepper, S., Swann, G. E. A., Thirumalai, K., Tierney, J. E., van der Weijst, C., White, S., Abe-Ouchi, A., Baatsen, M. L. J., Brady, E. C., Chan, W.-L., Chandan, D., Feng, R., Guo, C., von der Heydt, A. S., Hunter, S., Li, X., Lohmann, G., Nisancioglu, K. H., Otto-Bliesner, B. L., Peltier, W. R., Stepanek, C., and Zhang, Z.: Lessons from a high-CO2 world: an ocean view from $\sim$ 3 million years ago, Climate of the Past, 16, 1599–1615, https://doi.org/10.5194/cp-16-1599-2020, 2020.

Meier, W.N., Fetterer, F., Windnagel, A.K., and Stewart, S.: NOAA/NSIDC Climate Data Record of Passive Microwave Sea Ice Concentration, https://doi.org/https://doi.org/10.7265/efmz-2t65, 2021.

Meijers, A. J. S.: The Southern Ocean in the Coupled Model Intercomparison Project phase 5, Philosophical Transactions of the Royal Society A: Mathematical, Physical and Engineering Sciences, 372, 20130 296, https://doi.org/10.1098/rsta.2013.0296, 2014.

Mohrmann, M., Heuzé, C., and Swart, S.: Southern Ocean polynyas in CMIP6 models, The Cryosphere, 15, 4281–4313, https://doi.org/10.5194/tc-15-4281-2021, 2021.

Orsi, A. H., Johnson, G. C., and Bullister, J. L.: Circulation, mixing, and production of Antarctic Bottom Water, Progress in Oceanography, 43, 55–109, https://doi.org/10.1016/S0079-6611(99)00004-X, 1999.

Pagani, M., Liu, Z., LaRiviere, J., and Ravelo, A. C.: High Earth-system climate sensitivity determined from Pliocene carbon dioxide concentrations, Nature Geoscience, 3, 27–30, https://doi.org/10.1038/ngeo724, 2010.

Pattyn, F. and Morlighem, M.: The uncertain future of the Antarctic Ice Sheet, Science, 367, 1331–1335, https://doi.org/10.1126/science.aaz5487, 2020.

Peltier, W. R. and Vettoretti, G.: Dansgaard-Oeschger oscillations predicted in a comprehensive model of glacial climate: A “kicked” salt oscillator in the Atlantic, Geophysical Research Letters, 41, 7306–7313, https://doi.org/10.1002/2014GL061413, 2014.

Rintoul, S. R.: The global influence of localized dynamics in the Southern Ocean, Nature, 558, 209–218, https://doi.org/10.1038/s41586-018-0182-3, 2018.

Roquet, F., Madec, G., McDougall, T. J., and Barker, P. M.: Accurate polynomial expressions for the density and specific volume of seawater using the TEOS-10 standard, Ocean Modelling, 90, 29–43, https://doi.org/10.1016/j.ocemod.2015.04.002, 2015.

Rousselet, L., Cessi, P., and Forget, G.: Coupling of the mid-depth and abyssal components of the global overturning circulation according to a state estimate, Science Advances, 7, eabf5478, 2021.

Sallée, J.-B., Shuckburgh, E., Bruneau, N., Meijers, A. J. S., Bracegirdle, T. J., Wang, Z., and Roy, T.: Assessment of Southern Ocean water mass circulation and characteristics in CMIP5 models: Historical bias and forcing response, Journal of Geophysical Research: Oceans, 118, 1830–1844, https://doi.org/10.1002/jgrc.20135, 2013.

https://doi.org/10.5194/cp-2023-83
Preprint. Discussion started: 8 November 2023

Seki, O., Foster, G. L., Schmidt, D. N., Mackensen, A., Kawamura, K., and Pancost, R. D.: Alkenone and boron-based Pliocene pCO2 records, Earth and Planetary Science Letters, 292, 201–211, https://doi.org/10.1016/j.epsl.2010.01.037, 2010.

Sgubin, G., Swingedouw, D., Drijfhout, S., Mary, Y., and Bennabi, A.: Abrupt cooling over the North Atlantic in modern climate models, Nature Communications, 8, 14 375, https://doi.org/10.1038/ncomms14375, 2017.

Sherriff-Tadano, S., Abe-Ouchi, A., Yoshimori, M., Ohgaito, R., Vadsaria, T., Chan, W.-L., Hotta, H., Kikuchi, M., Kodama, T., Oka, A., and Suzuki, K.: Southern Ocean Surface Temperatures and Cloud Biases in Climate Models Connected to the Representation of Glacial Deep Ocean Circulation, Journal of Climate, 36, 3849–3866, https://doi.org/10.1175/JCLI-D-22-0221.1, 2023.

Sloyan, B. M. and Rintoul, S. R.: The Southern Ocean Limb of the Global Deep Overturning Circulation, Journal of Physical Oceanography, 31, 143–173, https://doi.org/10.1175/1520-0485(2001)031<0143:TSOLOT>2.0.CO;2, 2001.

Stepanek, C., Samakinwa, E., Knorr, G., and Lohmann, G.: Contribution of the coupled atmosphere–ocean–sea ice–vegetation model COSMOS to the PlioMIP2, Climate of the Past, 16, 2275–2323, https://doi.org/10.5194/cp-16-2275-2020, 2020.

Swart, N. C. and Fyfe, J. C.: Observed and simulated changes in the Southern Hemisphere surface westerly wind-stress, Geophysical Research Letters, 39, https://doi.org/10.1029/2012GL052810, 2012.

Talley, L. D.: Closure of the Global Overturning Circulation Through the Indian, Pacific, and Southern Oceans: Schematics and Transports, Oceanography, 26, 80–97, https://www.jstor.org/stable/24862019, 2013.

Tan, N., Contoux, C., Ramstein, G., Sun, Y., Dumas, C., Sepulchre, P., and Guo, Z.: Modeling a modern-like pCO2 warm period (Marine Isotope Stage KM5c) with two versions of an Institut Pierre Simon Laplace atmosphere–ocean coupled general circulation model, Climate of the Past, 16, 1–16, https://doi.org/10.5194/cp-16-1-2020, 2020.

Tjiputra, J. F., Assmann, K., and Heinze, C.: Anthropogenic carbon dynamics in the changing ocean, Ocean Science, 6, 605–614, https://doi.org/10.5194/os-6-605-2010, 2010.

Toggweiler, J. R. and Samuels, B.: Effect of drake passage on the global thermohaline circulation, Deep Sea Research Part I: Oceanographic Research Papers, 42, 477–500, https://doi.org/10.1016/0967-0637(95)00012-U, 1995.

von der Heydt, A. S., Dijkstra, H. A., van de Wal, R. S. W., Caballero, R., Crucifix, M., Foster, G. L., Huber, M., Köhler, P., Rohling, E., Valdes, P. J., Ashwin, P., Bathiany, S., Berends, T., van Bree, L. G. J., Ditlevsen, P., Ghil, M., Haywood, A. M., Katzav, J., Lohmann, G., Lohmann, J., Lucarini, V., Marzocchi, A., Pälike, H., Baroni, I. R., Simon, D., Sluijs, A., Stap, L. B., Tantet, A., Viebahn, J., and Ziegler, M.: Lessons on Climate Sensitivity From Past Climate Changes, Current Climate Change Reports, 2, 148–158, https://doi.org/10.1007/s40641-016-0049-3, 2016.

Wang, Y., Heywood, K. J., Stevens, D. P., and Damerell, G. M.: Seasonal extrema of sea surface temperature in CMIP6 models, Ocean Science, 18, 839–855, https://doi.org/10.5194/os-18-839-2022, 2022.

Weiffenbach, J. E., Baatsen, M. L. J., Dijkstra, H. A., von der Heydt, A. S., Abe-Ouchi, A., Brady, E. C., Chan, W.-L., Chandan, D., Chandler, M. A., Contoux, C., Feng, R., Guo, C., Han, Z., Haywood, A. M., Li, Q., Li, X., Lohmann, G., Lunt, D. J., Nisancioglu, K. H., Otto-Bliesner, B. L., Peltier, W. R., Ramstein, G., Sohl, L. E., Stepanek, C., Tan, N., Tindall, J. C., Williams, C. J. R., Zhang, Q., and Zhang, Z.: Unraveling the mechanisms and implications of a stronger mid-Pliocene Atlantic Meridional Overturning Circulation (AMOC) in PlioMIP2, Climate of the Past, 19, 61–85, https://doi.org/10.5194/cp-19-61-2023, 2023.

Whitehead, J., Wotherspoon, S., and Bohaty, S.: Minimal Antarctic sea ice during the Pliocene, Geology, 33, 137–140, https://doi.org/10.1130/G21013.1, 2005.

Whitehead, J. M. and Bohaty, S. M.: Pliocene summer sea surface temperature reconstruction using silicoflagellates from Southern Ocean ODP Site 1165, Paleoceanography, 18, 2003.

https://doi.org/10.5194/cp-2023-83
Preprint. Discussion started: 8 November 2023

Williams, C. J., Sellar, A. A., Ren, X., Haywood, A. M., Hopcroft, P., Hunter, S. J., Roberts, W. H., Smith, R. S., Stone, E. J., Tindall, J. C., and others: Simulation of the mid-Pliocene Warm Period using HadGEM3: experimental design and results from model–model and model–data comparison, Climate of the Past, 17, 2139–2163, https://doi.org/10.5194/cp-17-2139-2021, 2021.

Zhang, Q., Berntell, E., Axelsson, J., Chen, J., Han, Z., de Nooijer, W., Lu, Z., Li, Q., Zhang, Q., Wyser, K., and Yang, S.: Simulating the mid-Holocene, last interglacial and mid-Pliocene climate with EC-Earth3-LR, Geoscientific Model Development, 14, 1147–1169, https://doi.org/10.5194/gmd-14-1147-2021, 2021.

Zhang, Q., Liu, B., Li, S., and Zhou, T.: Understanding Models' Global Sea Surface Temperature Bias in Mean State: From CMIP5 to CMIP6, Geophysical Research Letters, 50, e2022GL100 888, https://doi.org/10.1029/2022GL100888, 2023.

Zunz, V., Goosse, H., and Massonnet, F.: How does internal variability influence the ability of CMIP5 models to reproduce the recent trend in Southern Ocean sea ice extent?, The Cryosphere, 7, 451–468, https://doi.org/10.5194/tc-7-451-2013, 2013.